Int J Adv Manuf Technol (2017) 93:1989–1997
DOI 10.1007/s00170-017-0639-9

ORIGINAL ARTICLE

A study of the grinding performance of laser micro-structured coarse-grained diamond grinding wheels

Hui Deng[1] · **Jie He**[2]

Received: 11 January 2017 / Accepted: 5 June 2017 / Published online: 23 June 2017

Abstract Considering the relatively poor surface and subsurface quality of workpieces that are ground by coarse-grained grinding wheels, the nanosecond ultraviolet laser micro-structuring of coarse-grained diamond grinding wheels and the grinding performance of micro-structured grinding wheels were investigated in this study. In addition, the effect of two processing sequences on the topographical characteristics of the grooves and the effect of the groove angle (α) on the surface roughness (R_a) of the ground workpiece were explored. Furthermore, the surface quality of workpieces that were ground by micro-structured (V-shaped and W-shaped patterns) and non-structured diamond grinding wheels and the grinding ratio (G) of the grinding wheels were comparatively analyzed. The results demonstrate the following: Compared with the grinding wheel that was subjected to micro-structuring followed by sharpening, the surface of the grinding wheel that was subjected to sharpening followed by micro-structuring had a more integral groove structure. Neither an overly large α nor an overly small α was favorable for improving the surface quality of the workpiece that was ground by a micro-structured grinding wheel. When $\alpha = 60°$, the minimum R_a of the workpiece was attained. The R_a of the workpieces that were ground by the grinding wheel with a V-shaped pattern (grinding wheel A) was 17–31% less than the R_a of the workpieces that were ground by the non-structured grinding wheel (grinding wheel C). The R_a of the workpieces that were ground by the grinding wheel with a W-shaped pattern (grinding wheel B) was 32–41% less than the R_a of the workpieces that were ground by grinding wheel C. The grinding performance of the micro-structured grinding wheels was related not only to the geometric parameters of the grooves but also to the micro-structure pattern. The W-shaped pattern was superior to the V-shaped pattern in terms of cooling and chip removal. Grinding wheel A and grinding wheel B had similar abrasion resistance, which were 26% less and 23% less than the abrasion resistance of grinding wheel C, respectively.

Keywords Coarse-grained diamond grinding wheel · Laser micro-structuring · Ground surface quality · Grinding ratio · Micro-structured pattern

1 Introduction

For cemented carbides, engineering ceramics, optical glasses, and other hard and brittle materials that are widely used in machinery, national defense, aerospace, and other fields, a fine or powder diamond wheel with grain sizes of microns or even submicrons is still the most effective and practical processing tool for precision and ultra-precision machining [1]. However, this type of grinding wheel has some troublesome drawbacks: a small chip space and a low bond-to-abrasive retaining strength. Clogging of the wheel surface, grains falling off easily, and needing frequent time-consuming dressing during grinding all result from these drawbacks [2]. Therefore, the processing cost for hard brittle materials is high, and the superabrasive is greatly wasted; thus, the precision machining of hard and brittle materials is neither economic nor green.

However, coarse-grained grinding wheels have advantages such as a large chip space and a strong bond-holding force [3].

✉ Hui Deng
denghnu@163.com

[1] Intelligent Manufacturing Institute, Hunan University of Science and Technology, Xiangtan 411201, China

[2] Sheet Metal Division, Han's Laser Technology Industry Group Company Limited, Shenzhen 518052, China

Therefore, in recent years, feasibility studies have been conducted using coarse-grained diamond wheel for precision and ultra-precision machining of hard and brittle materials. For example, Zhao [4, 5] et al. developed a monolayer electroplated diamond grinding wheel after precisely dressing with grain sizes of 46, 91, and 151 μm (with a peak height difference for the grains of less than 2.5 μm); in this way, precision machining of BK7 and SF6 optical glass was achieved. The R_a of the ground workpiece can reach the nanometer level. However, the subsurface damage depth (SSD) of ground optical glass has been found to have the following relationship with the grain diameter d: $0.3d^{0.68} < \mathrm{SSD}(\mu m) < 2d^{0.85}$ [6]. That is, with increasing grain size, the SSD of the workpiece after grinding increases. The reasons for this are described as follows: A grain has a truncated octahedral shape (Fig. 1a). After dressing, its top is cut to a facet (Fig. 1b), and the area of the facet increases with increasing grain size, which increases the contact area between the grain and workpiece during grinding. Therefore, the cooling liquid cannot easily reach the grinding area. This increases the normal grinding force and the grinding temperature, eventually resulting in increased SSD of the workpiece after grinding.

To solve this problem, a nanosecond ultraviolet laser beam will be used to cut micron-sized grooves on the surfaces of diamond grains (i.e., laser structuring grinding wheel), as shown in Fig. 1c. This process sought to reduce the contact area of the grain-workpiece and to increase the number of effective cutting edges on the wheel surface. The goal is to improve the surface quality of the workpiece after grinding. Laser structuring is one of the methods used to make a structured wheel. A laser beam is used to produce a regular arrangement of grooves or holes on the grinding wheel's surface [7, 8], as shown in Fig. 2. Depending on the groove width (or hole diameter), laser structuring can be subdivided into macro-structuring (>100 μm) and micro-structuring (<100 μm) [9]. Laser macro-structuring is primarily used to machine fine-grained grinding wheels with a groove width that is substantially greater than the grain diameter (The number of effective grains on the surface of a grinding wheel is considerably decreased after the grinding wheel is subjected to macro-structuring). This process aims to reduce the contact area between the grinding wheel and the workpiece and increase the chip space of the grinding wheel surface. Laser micro-structuring is primarily used to machine coarse-grained grinding wheels with a groove width that is less than the grain diameter. This process aims to reduce the contact area between the grains and the workpiece and increase the number of effective cutting edges on the grinding wheel surface without reducing the number of effective grains. Thus, the surface and subsurface qualities of the ground workpiece are improved.

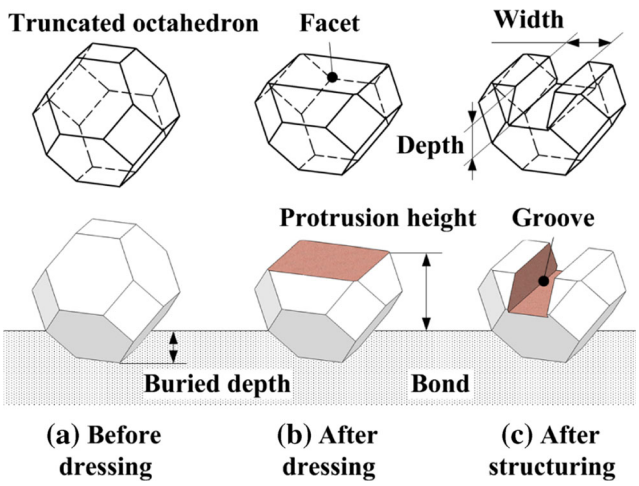

Fig. 1 Shape of grains

Currently, the laser micro-structuring of coarse-grained grinding wheels has been studied by only a few researchers. A pulsed laser beam was used by Guo et al. [10, 11] to produce linear grooves with a width (w) of 10–15 μm; a spacing (s) of 30, 70, 90, and 150 μm; and an angle between the axis of the grinding wheel and groove direction (α) of 90° on the surface of a single-layer electroplated diamond wheel with a grain diameter (d) of 150 μm. BK7 optical glass was then ground at a wheel speed of 3000 r/min, a feed speed of 2 mm/min, and a grinding depth of 2 μm. Compared with a non-structured wheel, the micro-structured wheel reduced the SSD of ground optical glass by 2–3 μm, and the damage depth decreased with decreasing groove spacing. However, because the groove direction of each of the previously mentioned structured grinding wheels is vertical to its axis, the cross-sectional shape of the grooves can be easily copied onto the optical glass surface. As a result, the R_a of a workpiece that is ground by each of the previously mentioned structured grinding wheels is greater than the R_a of a workpiece that was ground by a non-structured grinding wheel. In addition, the R_a of a workpiece that was ground by each of the previously mentioned structured grinding wheels significantly increases with increasing groove spacing.

Therefore, the effect of the processing sequence on the topographical characteristics of the grooves and the effect of the groove angle on the surface roughness of the ground workpiece will be investigated in this study. Based on this study, two types of micro-structured diamond grinding wheels with different patterns (V-shaped and W-shaped patterns) will be fabricated. Finally, YG8 cemented carbide workpieces will be ground using the fabricated micro-structured grinding wheels and a non-structured grinding wheel, and the surface quality of the ground workpieces and the grinding ratio of the grinding wheels will be comparatively analyzed.

2 Experimental conditions

The bronze-bonded diamond grinding wheels that were used in the experiment had a diameter (D) of 100 mm, a width (W)

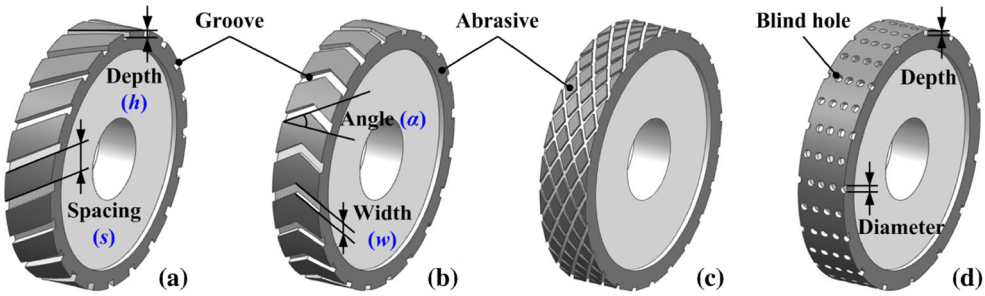

Fig. 2 Laser structured grinding wheel with different patterns. **a** helix. **b** cross-helix. **c** V-large. **d** hole

of 10 mm, and a grain size (d) of 250 μm, as shown in Fig. 3a, b. Tungsten–cobalt cemented carbide blocks that consist of tungsten carbide (content: 92%) and cobalt (content: 8%) (YG8) were selected as the workpieces for grinding, as shown in Fig. 3c.

After each set of experiments, the surface topography of the grinding wheel and the workpiece as well as the surface roughness of the workpiece were observed using a video microscope (HG-918C), a 3D optical microscope with an ultra-deep depth of field (VHX-S1000) and a roughness tester (JB-4C) (sample length was 0.8 mm, evaluation length was 4 mm; the measurement direction was perpendicular to the grinding direction; the value of the roughness of the grinded surface was taken as the average roughness of three different positions on the surface).

3 Micro-structured grinding wheels

3.1 Devices and parameters

The experimental device that was used for the nanosecond ultraviolet laser (pulse width 18 ns, wavelength 355 nm) micro-structuring of the grinding wheels is shown in Fig. 4a. The working principle of the galvanometer scanning system with a front objective lens that was used in the experiment is shown in Fig. 4b. The laser beam (average power P_{avg} = 4.5–7.5 W, pulse frequency f = 30 kHz, scanning speed v = 800 mm/s) was successively passed through the expander, the X and Y galvanometer and the focus lens before finally impinging on the surface of the grinding wheel installed at the main axis of the surface grinder (MGS-250AH) with a defocus (Δ) of 0 mm and a focal spot diameter (d_f) of 35 μm. To ensure that the diameter of the laser beam irradiating on the cylindrical surface of the wheel is consistent (i.e., defocus invariant), the wheel's central angle was divided equally. When the arc surface corresponding to an angle θ was completed, the wheel was rotated by θ along a fixed direction for continued processing until the micro-structuring of the entire wheel surface was complete (groove width w = 75.3 μm, groove depth h = 38.2 μm, groove spacing s = 174.7 μm). Accurate grinding wheel angle control can be achieved by the main axis of the grinder spindle with a precision up to 0.1°.

3.2 Processing sequences

The surface topography of the grinding wheel that was subjected to laser profiling followed by laser sharpening is shown in Fig. 5a. The surface topography of the grinding wheel that was subjected to laser profiling followed by laser micro-structuring and sharpening is shown in Fig. 5b. The surface topography of the grinding wheel that was subjected to laser profiling followed by laser sharpening and micro-structuring is shown in Fig. 5c.

The groove structure on the surface of the grinding wheel that was subjected to micro-structuring followed by sharpening was lost. This occurred because the grooves on the surface of the bond had a depth of approximately 100 μm after micro-structuring. In addition, to enable the protrusion height of the grains to reach 1/3 of their diameter (d), the bond surrounding the grains was removed to a depth of approximately 83 μm during the sharpening process. Consequently, the groove structure was significantly damaged. The integrity of the groove structure on the surface of the grinding wheel that was subjected to sharpening followed by micro-structuring

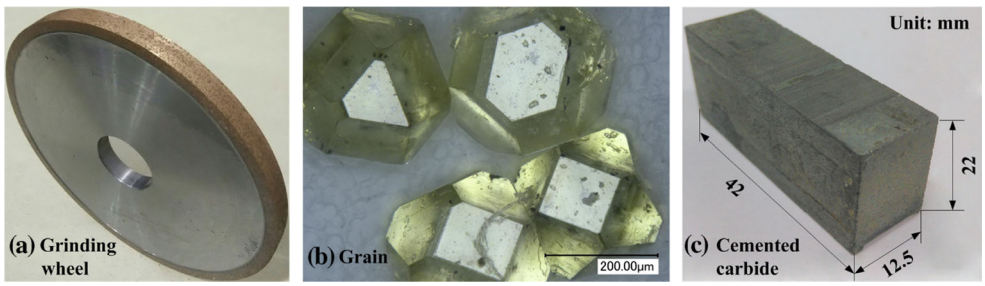

Fig. 3 Bronze-bonded diamond grinding wheel and cemented carbide workpiece

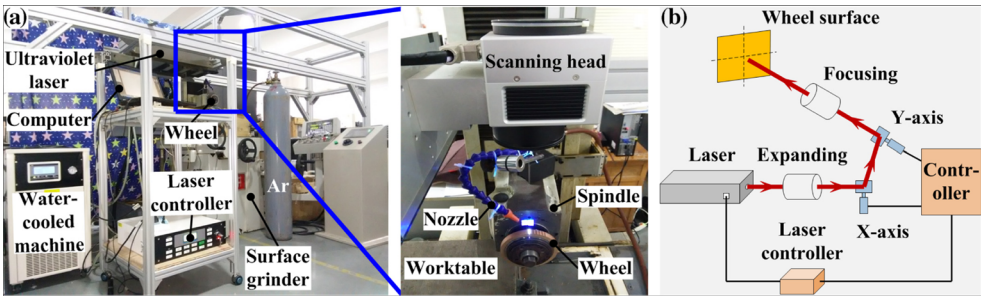

Fig. 4 Experimental apparatus used for laser micro-structuring. **a** laser micro-structuring device. **b** working principle of galvanometer

was maintained. Therefore, the grinding wheel processing sequence, in which the grinding wheel was subjected to profiling followed by sharpening and micro-structuring, was subsequently followed.

3.3 Groove angle

The groove angle (α) can affect both the cutting angle of a grain cutting edge and the distribution of coolant in the grinding area, thus influencing the surface quality of the workpiece. Laser micro-structuring experiments were conducted on the surfaces of four grinding wheels with different groove angles. The surface topographies of the micro-structured grinding wheels are shown in Fig. 6.

The micro-structured grinding wheels were used to up-grind the YG8 cemented carbide workpiece without cooling liquid; the observed results of the surface roughness R_a and surface topography of the post-grinding workpieces are shown in Fig. 7. As shown in this figure, when α is 0°, the groove direction is perpendicular to the direction of the workpiece feeding. The contact between the workpiece and the grinding wheel during grinding is intermittent, thereby increasing the impact and vibration between the wheel and workpiece and resulting in poor workpiece surface quality (R_a = 2.53 μm). When α is 90°, the groove direction is the same as the workpiece feed direction. In this case, the groove shape is easily reflected onto the surface of the workpiece during grinding, and the workpiece surface quality is also not ideal (R_a = 2.82 μm). These results suggest that a groove angle that is too small or too large is not helpful for improving the workpiece surface roughness after grinding by micro-structured wheel. When α is 30° or 60°, a continuous grinding process is ensured, and the groove shape is not easily reflected onto the surface of the workpiece, thus achieving better workpiece surface quality. Under these conditions, R_a reaches a minimum value of 1.56 μm when α is 60°.

3.4 Grinding wheel fabrication

A processing sequence in which the grinding wheel was subjected to sharpening followed by micro-structuring was employed. When the groove angle (α) was set to 60°, the surfaces of the two grinding wheels were subjected to laser micro-structuring to introduce different patterns. The surface topography of the two micro-structured grinding wheels—A and B—that were fabricated in this study are shown in Fig. 8. Grinding wheel A was given a V-shaped pattern, whereas grinding B was given a W-shaped pattern. As shown in this figure, one and only one groove is found on the surface of most of the grains, i.e., the majority of the grains on the grinding wheel surface had two cutting edges.

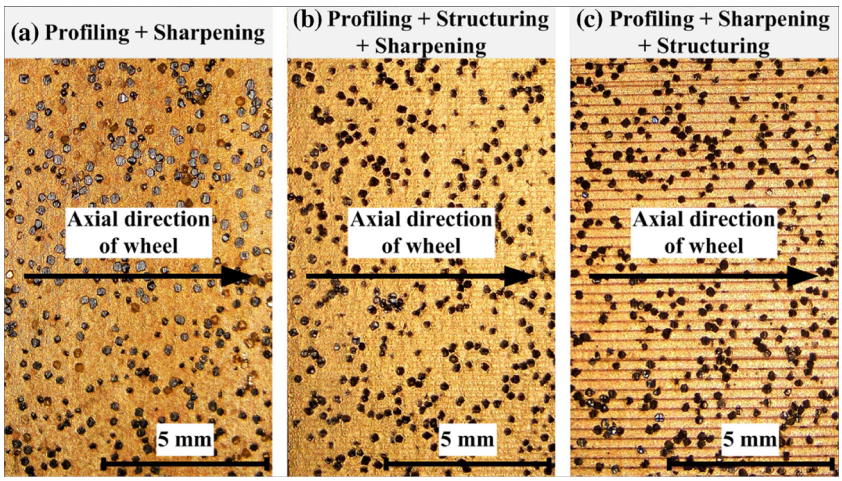

Fig. 5 Surface topography of the grinding wheels subjected to different processing sequences

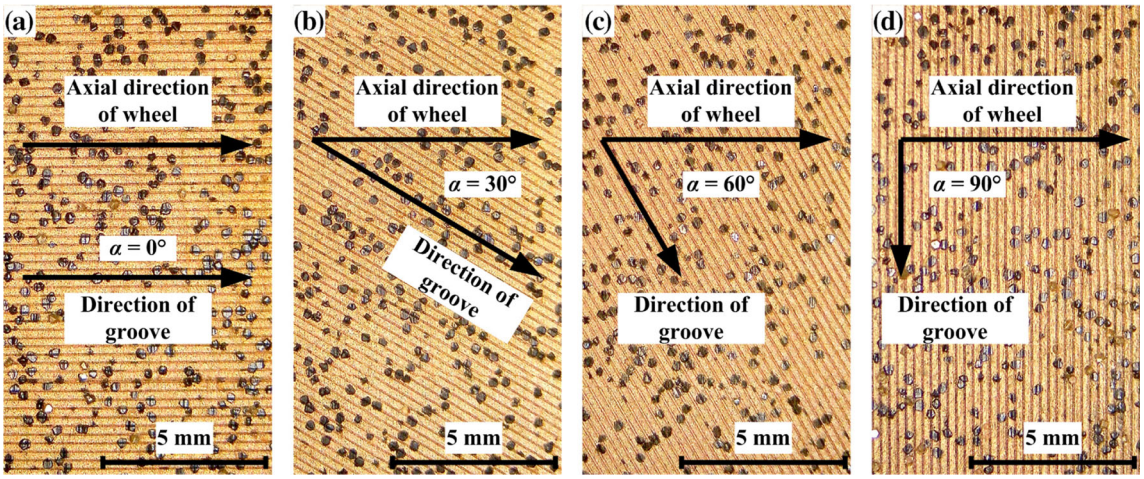

Fig. 6 Surface topographies of micro-structured grinding wheels with different groove angles. **a** $\alpha = 0°$. **b** $\alpha = 30°$. **c** $\alpha = 60°$ *d* $\alpha = 90°$

4 Workpiece surface quality

4.1 Devices and parameters

Cemented carbide workpieces were subjected to reciprocating flat surface grinding on a surface grinder with a horizontal spindle and a rectangular table (SL800A/1-HZ) (Fig. 9a) using grinding wheels A, grinding wheel B, or a non-structured grinding wheel (grinding wheel C) (Fig. 5a). The experimental scheme and experimental parameters are shown in Fig. 9b, c, respectively.

4.2 Micro-topography

Fig. 10 shows the surface topography of each ground cemented carbide workpiece. A large number of micro-scratches on the ground surface were generated by the gliding of the grains. For the same parameter conditions, the scratches on the surface of the workpiece that was ground by grinding wheels A and B were narrower, shallower, and more evenly distributed than the scratches on the surface of the workpiece that was ground by grinding wheel C. The reasons are as follows: Compared with the non-structured grinding wheel, most of the grains on the surface of each of the micro-structured grinding wheels had two cutting edges. The non-structured grinding wheel and the two micro-structured grinding wheels had the same number of grains, but the number of cutting edges on the surface of each micro-structured grinding wheel was almost twice the number of cutting edges on the surface of the non-structured grinding wheel. In addition, the ground surface was formed with innumerable micro-scratches, which were produced by the cutting edges of the grains. Consequently, a greater number of

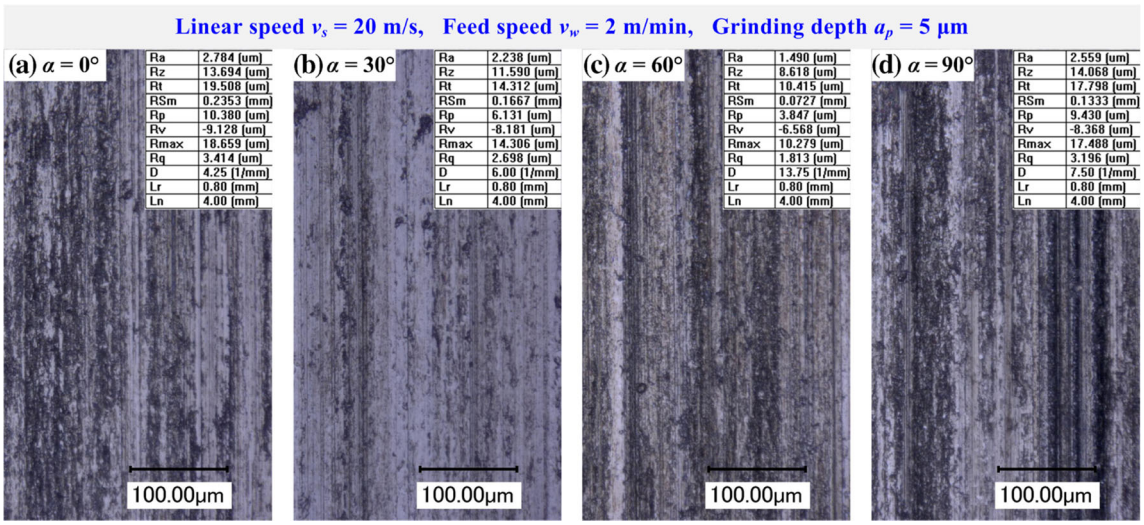

Fig. 7 Surface topography and roughness of the workpieces

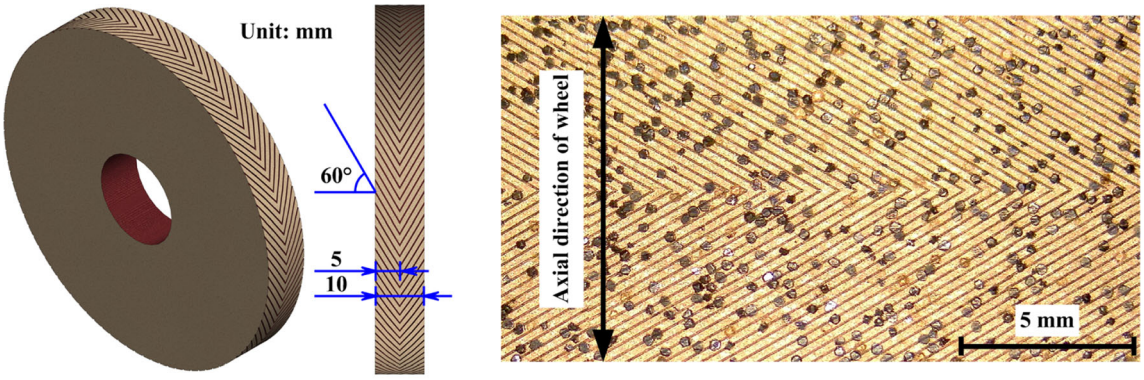

Fig. 8 Surface topography of the micro-structured grinding wheels with different patterns

grains participated in machining the grinding wheel (i.e., a greater number of scratches per unit area of the workpiece) and a more consistent grain protrusion height (i.e., a more consistent height of the scratches) resulted in narrower, shallower, and more even scratches made by the grains when they passed the grinding region.

4.3 Surface roughness

The surface roughness measurements of the workpieces that were ground at different parameter conditions are shown in Fig. 11. The surface roughness (R_a) of the workpiece decreased with increasing linear speed of the grinding wheel (v_s) and increased with increasing workpiece feed speed (v_w). When v_s = 21 m/s and v_w = 1 m/min, the minimum R_a of the workpiece that was ground by grinding wheels A, B, and C was attained (1.002, 0.703, and 0.623 μm, respectively). The surface topography of the workpieces is shown in Fig. 10b. A decrease in v_s or an increase in v_w increased the maximum undeformed chip thickness of a single grain (h_{max}). In Eq. (1) [12], C_a represents the number of cutting edges of the effective

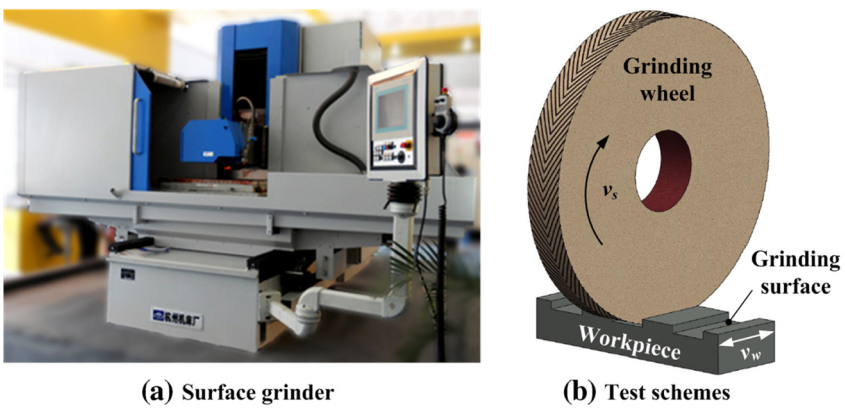

(a) Surface grinder (b) Test schemes

Linear speed, v_s	9–21 m/s
Feed speed, v_w	1–4 m/min
Grinding depth, a_p	3 μm
Grinding fluid	40 L/min
Workpiece dimension	42×12.5 ×22 mm

(c) Test parameters

Fig. 9 Experimental scheme and parameters

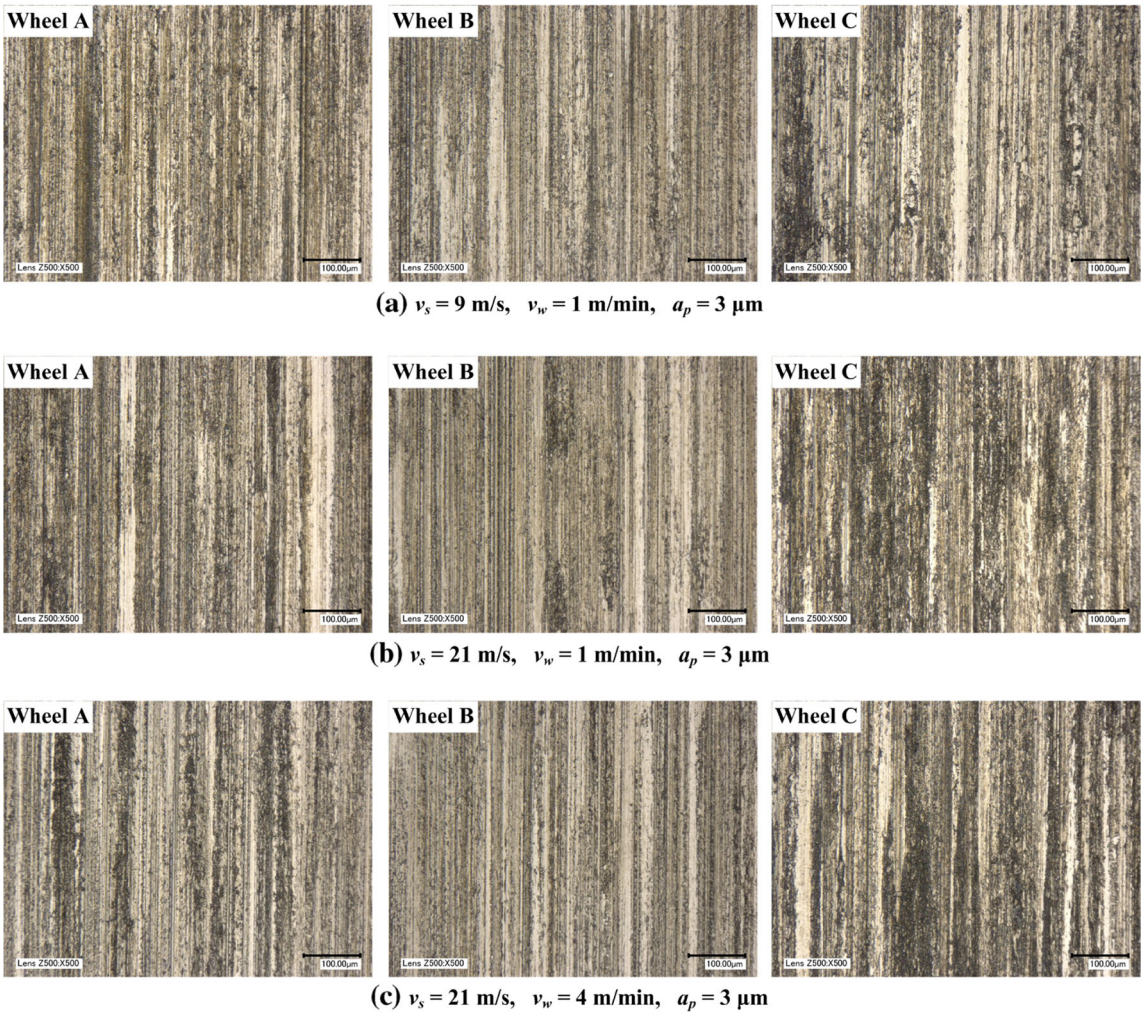

Fig. 10 Surface micro-topography of the ground workpieces

grains within the unit surface area of the grinding wheel, and β represents half of the cone apex angle of a grain. In addition, a decrease in v_s or an increase in v_w increased the arc length of the contact line between the grinding wheel and the workpiece when they were in motion (l_k). In Eq. (2) [12], "+" signifies up-grinding and "–" signifies down-grinding. An increased maximum undeformed chip thickness or an increased arc length increases the grinding force, the grinding zone temperature during the grinding process and the R_a of the ground workpiece.

$$h_{\max} = \left(\frac{3}{C_a \tan\beta}\right)^{\frac{1}{2}} \left(\frac{v_w}{v_s}\right)^{\frac{1}{2}} \left(\frac{a_p}{D}\right)^{\frac{1}{4}} \tag{1}$$

$$l_k = \left(1 \pm \frac{v_w}{60 v_s}\right) (a_p D)^{\frac{1}{2}} \tag{2}$$

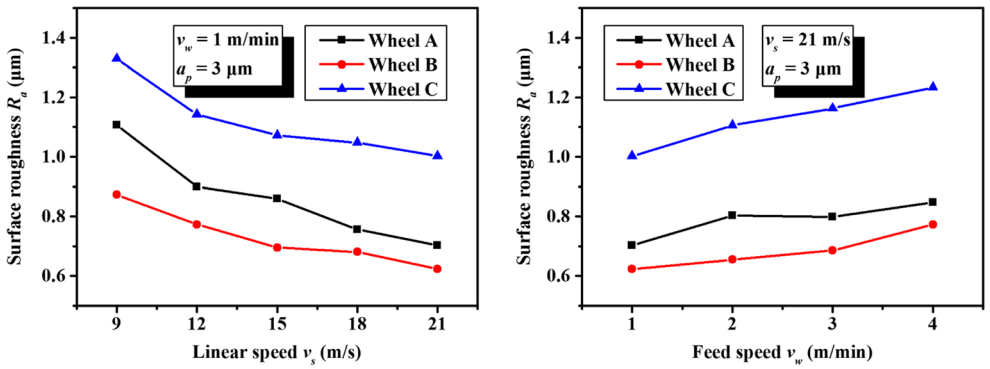

Fig. 11 Surface roughness of the ground workpiece

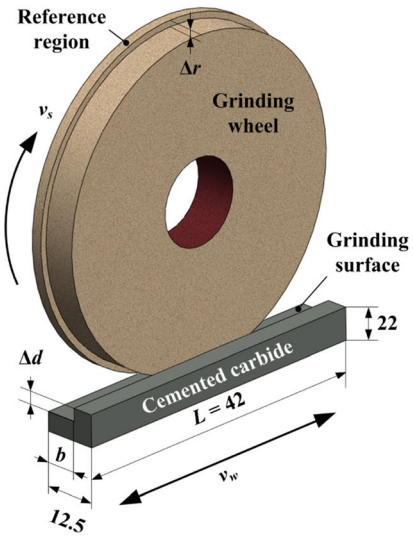

(a) Test schemes

Linear speed, v_s	21 m/s
Feed speed, v_w	1 m/min
Grinding depth, a_p	3 μm
Accumulated grinding depth, Δd	20 mm
Grinding fluid	40 L/min
Workpiece dimension	42×12.5×22 mm

(b) Test parameters

Fig. 12 Experimental scheme and parameters

In equivalent parameter conditions, the surface roughness (R_a) of the workpiece that was ground by grinding wheel C was the highest, followed by the R_a of the workpiece ground by grinding wheel A, which was 17–31% less than the R_a of the workpiece that was ground by grinding wheel C, and the R_a of the workpiece that was ground by grinding wheel B, which was 32–41% less than the R_a of the workpiece that was ground by grinding wheel C. The reasons are as follows: compared with the non-structured grinding wheel, the grooves on the surface of each micro-structured grinding wheel were more favorable to the cooling and chip removal effect of the grinding fluid. In addition, the majority of the grains on the surface of each micro-structured grinding wheel had two cutting edges (i.e., a larger C_a and a smaller h_{max} in Eq. (2)). As a result, the surface quality of the workpiece that was ground by either grinding wheel A or B was better than the surface quality of the workpiece that was ground by grinding wheel C. The grooves on the surfaces of grinding wheels A and B had the same geometric parameters (width, depth, spacing and angle). However, the R_a of the workpiece that was ground by grinding wheel B was less than the R_a of the workpiece that was ground by grinding wheel A, which indicated that the grinding performance of the micro-structured grinding wheels was related not only to the geometric parameters of the grooves but also to the micro-structure pattern, and the W-shaped pattern was superior to the V-shaped pattern in cooling and chip removal.

5 Grinding ratio of the grinding wheels

5.1 Devices and parameters

Three cemented carbide workpieces were subjected to reciprocating flat surface grinding on a surface grinder with a horizontal spindle and a rectangular table using grinding wheels A, B, and C. The experimental scheme and parameters are shown in Fig. 12. In each set of experiments, only 7.5 mm (widthwise) of the grinding wheel surface was used to grind the workpiece, and the experiment was terminated when a cumulative grinding depth (Δd) of 20 mm was attained. The remaining 2.5 mm (widthwise) of the grinding wheel surface was used as the reference region to determine the change in the surface topography of the grinding wheel after the grinding process.

5.2 Grinding ratio

In the practical production process, the grinding ratio (G) is often used as an important index to characterize the abrasion resistance of a grinding wheel. A greater value of G increases the volume of the workpiece material removed by grinding per unit volume of the grinding wheel worn and also increases the abrasion resistance of the grinding wheel. G is the ratio of the volume of the workpiece per unit width that was removed by grinding (V_w) to the volume of the grinding wheel worn per unit width (V_s). For flat surface grinding, G is expressed as

$$G = \frac{V_w}{V_s} = \frac{L\Delta d}{\pi\left(R^2-(R-\Delta r)^2\right)} = \frac{L\Delta d}{\pi(2R\Delta r-\Delta r^2)} \quad (3)$$

where L represents the length of the cemented carbide workpiece (L = 42 mm in this study), Δd represents the cumulative grinding depth (Δd = 20 mm in this study), R represents the initial radius of the grinding wheel (R = 75 mm in this study), and Δr represents the decrease in the radius of the grinding wheel. A grinding wheel has a complex surface topography, and the Δr after the grinding process is substantially smaller

than R. Therefore, relatively large errors will be introduced if Δr is directly measured using tools such as a micrometer caliper and a vernier caliper. In this study, the decrease in the protrusion height of the grains after the grinding process was used to characterize Δr.

In all three sets of experiments, Δd = 20 mm. The V_w in each set of experiments was obtained via calculations; V_w is 840 mm^3/mm in all three sets of experiments. The grain height on the grinding wheel surface that had participated in the grinding process and had not participated in the grinding process in each set of experiments was measured using a 3D optical microscopy with an ultra-deep depth of field. The results indicated that Δr was approximately 4.35, 4.21, and 3.24 μm for grinding wheels A, B, and C, respectively. The V_s in each set of experiment was obtained via calculations; V_s is 1.37, 1.32, and 1.02 mm^3/mm) for grinding wheels A, B, and C, respectively. By substituting the value of V_w and V_s into Eq. (3), the values of G of grinding wheel A, B, and C were obtained: G = 614.7, 635.1, and 825.3, respectively. Grinding wheels A and B had similar abrasion resistance. Compared with the non-structured grinding wheel, the edges of the grooves that pass through the grains on the surface of each micro-structured grinding wheel were relatively more susceptible to wear. As a result, the abrasion resistance of grinding wheel A and grinding wheel B were 26% less and 23% less than the abrasion resistance of grinding wheel C, respectively.

6 Conclusions

The effect of two processing sequences on the topographical characteristics of the grooves and the effect of the groove angle on the surface roughness of the ground workpiece were investigated in this study. In addition, the surface quality of the workpieces that were ground by micro-structured (V-shaped and W-shaped patterns) and non-structured diamond grinding wheels and the grinding ratio of the grinding wheels were comparatively analyzed. The main conclusions are presented as follows: Compared with the grinding wheel that was subjected to micro-structuring followed by sharpening, the surface of the grinding wheel that was subjected to sharpening followed by micro-structuring had a more integral groove structure. Neither an overly large groove angle (α) nor an overly small groove angle was favorable for improving the surface roughness (R_a) of the workpiece that was ground by each micro-structured grinding wheel. When α = 60°, the maximum R_a was attained (1.56 μm). The R_a of the workpiece that was ground by the micro-structured grinding wheel with a V-shaped pattern (grinding wheel A) was 17–31% less than the R_a of the workpiece that was ground by the non-structured grinding wheel (grinding wheel C). The R_a of the workpiece that was ground by the micro-structured grinding wheel with a W-shaped pattern (grinding wheel B) was 32–41% less than the R_a of the workpiece that was ground by grinding wheel C. The grinding performance of the micro-structured grinding wheels was related not only to the geometric parameters of the grooves but also to the micro-structure pattern. The W-shaped pattern was superior to the V-shaped pattern in terms of cooling and chip removal. Grinding wheels A and B had similar abrasion resistances, which were 26% and 23% less than the abrasion resistance of grinding wheel C, respectively.

Acknowledgments Financial support for this research was provided by the National Natural Science Foundation of China (No. 51605162) and the Hunan Provincial Natural Science Foundation of China (No. 2017JJ3077).

References

1. Brinksmeier E, Mutluguenes Y, Klocke F, Aurich JC, Shore P, Ohmori H (2010) Ultra-precision grinding. CIRP Ann-Manuf Techn 59:652–671. doi:10.1016/j.cirp.2010.05.001
2. Heinzel C, Rickens K, Trumpold H (2009) Engineered wheels for grinding of optical glass. CIRP Ann-Manuf Techn 58:315–318. doi:10.1016/j.cirp.2009.03.096
3. Lu YJ, Xie J, Si XH (2015) Study on micro-topographical removals of diamond grain and metal bond in dry electro-contact discharge dressing of coarse diamond grinding wheel. Int J Mach Tool Manu 88:118–130. doi:10.1016/j.ijmachtools.2014.09.008
4. Zhao Q, Guo B (2015) Ultra-precision grinding of optical glasses using mono-layer nickel electroplated coarse-grained diamond wheels. Part 2: investigation of profile and surface grinding. Precis Eng 39:67–78. doi:10.1016/j.precisioneng.2014.07.007
5. Zhao Q, Guo B (2015) Ultra-precision grinding of optical glasses using mono-layer nickel electroplated coarse-grained diamond wheels. Part 1: ELID assisted precision conditioning of grinding wheels. Precis Eng 39:56–66. doi:10.1016/j.precisioneng.2014.07.006
6. Aida H, Takeda H, Kim S, Aota N, Koyama K, Yamazaki T, Doi T (2014) Evaluation of subsurface damage in GaN substrate induced by mechanical polishing with diamond abrasives. Appl Surf Sci 292:531–536. doi:10.1016/j.apsusc.2013.12.005
7. Walter C, Komischke T, Kuster F, Wegener K (2014) Laser-structured grinding tools—generation of prototype patterns and performance evaluation. J Mater Process Tech 214:951–961. doi:10.1016/j.jmatprotec.2013.11.015
8. Khangar A, Dahotre NB (2005) Morphological modification in laser-dressed alumina grinding wheel material for microscale grinding. J Mater Process Tech 170:1–10. doi:10.1016/j.jmatprotec.2005.04.087
9. Li HN, Axinte D (2016) Textured grinding wheels: a review. Int J Mach Tool Manu 109:8–35. doi:10.1016/j.ijmachtools.2016.07.001
10. Guo B, Zhao Q, Fang X (2014) Precision grinding of optical glass with laser micro-structured coarse-grained diamond wheels. J Mater Process Tech 214:1045–1051. doi:10.1016/j.jmatprotec.2013.12.013
11. Guo B, Zhao Q, Yu X (2014) Surface micro-structuring of coarse-grained diamond wheels by nanosecond pulsed laser for improving grinding performance. Int J Precis Eng Man 15:2025–2030. doi:10.1007/s12541-014-0559-7
12. Deng H, Deng Z, Li S (2017) The grinding performance of a laser-dressed bronze-bonded diamond grinding wheel. Int J Adv Manuf Tech 88:1789–1798. doi:10.1007/s00170-016-8902-z